Effects of energetic disorder on the low-frequency differential capacitance of organic light emitting diodes

AIP | Journal of Applied Physics

Effects of energetic disorder on the low-frequency differential capacitance of organic light emitting diodes

W. C. Germs, S. L. M. van Mensfoort, R. J. de Vries, and R. Coehoorn

Citation: J. Appl. Phys. **111**, 074506 (2012); doi: 10.1063/1.3701575
View online: http://dx.doi.org/10.1063/1.3701575
View Table of Contents: http://jap.aip.org/resource/1/JAPIAU/v111/i7
Published by the American Institute of Physics.

Effects of energetic disorder on the low-frequency differential capacitance of organic light emitting diodes

W. C. Germs,[1,2,a)] S. L. M. van Mensfoort,[1,2] R. J. de Vries,[1,2,3] and R. Coehoorn[1,2]
[1]*Molecular Materials and Nanosystems, Department of Applied Physics, Eindhoven University of Technology, P.O. Box 513, 5600 MB Eindhoven, The Netherlands*
[2]*Philips Research Laboratories, High Tech Campus 4, 5656 AE Eindhoven, The Netherlands*
[3]*Dutch Polymer Institute (DPI), P.O. Box 902, 5600 AX Eindhoven, The Netherlands*

(Received 4 November 2011; accepted 20 February 2012; published online 6 April 2012)

It has recently been shown how the injection barriers at the electrode interfaces and the built-in voltage (V_{bi}) of organic light emitting diodes can be obtained from measurements of the differential capacitance at low frequencies, using the voltage and height of a distinct peak in the capacitance-voltages curves. In this paper, we investigate the effects of Gaussian energetic disorder on the analysis, for single-carrier and double-carrier devices. We show how the disorder affects the peak position and height, and how from combined capacitance-voltage measurements and device modeling the injection barriers and V_{bi} can be determined. As examples, hole-only and double-carrier devices are investigated based on a blue-emitting polyfluorene-triarylamine copolymer. © *2012 American Institute of Physics*. [http://dx.doi.org/10.1063/1.3701575]

I. INTRODUCTION

Measurements of the differential capacitance of single-layer organic light emitting diodes (OLEDs) have been employed to determine the electron and hole mobilities in the organic semiconductor material[1] and the energy barriers at the two electrode interfaces.[2] Within these studies, use is made of the frequency (f) dependence of the differential capacitance (C), around frequencies corresponding to the inverse charge carrier transit time, and of the low-frequency voltage (V) dependence of the capacitance, respectively. In this paper, we focus on the latter type of study. In Ref. 2, an analysis of low-frequency $C(V)$ measurements to determine the injection barriers was carried out assuming a constant mobility and diffusion coefficient, and for single-carrier devices only. It is the purpose of this paper to analyze how the application of $C(V)$ measurements as a non-invasive technique for determining the energy barriers as well as the built-in voltage, V_{bi}, can be extended to single-carrier and double-carrier devices based on disordered organic semiconductors with a spatially uncorrelated Gaussian density of states. The charge carrier mobilities depend then on the charge carrier density and on the electric field.[3–5]

The method makes use of the occurrence of a distinct low-frequency peak in the differential capacitance, which is observed when the energy barrier at the injecting contact is relatively small. In Fig. 1, the thick curves ("no disorder") show the $C(V)$ curves of a single layer OLED for the case of a constant mobility and diffusion coefficient and with no injection barriers, already given in Ref. 2. For symmetric devices, with $V_{bi} = 0\,V$, the peak in the capacitance is situated at $V = 0\,V$ (Fig. 1(a)). The effect may be understood as a result of charge carrier diffusion, which already at zero voltage leads to an appreciable space charge near the electrodes. This effectively lowers the distance between the electrode planes, so that the capacitance is larger than the geometrical capacitance, $C_{geom} = \varepsilon/L$, with ε the electric permittivity of the organic semiconductor and L the layer thickness. Upon the application of a voltage, the space charge in the bulk of the device increases. The finite charge-carrier transit time gives rise to a delayed response of this bulk space charge distribution to an applied voltage change, leading to a negative contribution to the capacitance. This is the predominant effect at high voltages, when the drift-contribution to the current density is much more important than the diffusion-contribution. For the case of a system with ideal contacts, the peak height is $C_{peak}/C_{geom} = 1.29$.[6] The peak half-width, defined as the voltage at which $C = C_{geom}$, is equal to $16k_BT/e$. This may be viewed as the crossover voltage between diffusion-dominated and drift-dominated ac transport. It follows from analytical drift-only theory that for high voltages the low-frequency differential capacitance is equal to $(3/4)C_{geom}$.[7]

For asymmetric devices, with a finite value of V_{bi}, the formation of a significant space charge layer near the injecting electrode sets in above zero voltage, but already well below V_{bi}. The peak voltage, V_{peak}, may be several tenths of a volt smaller than V_{bi}, depending on the injection barrier at the injecting contact. With increasing injection barrier, the peak shifts to V_{bi}, and the intensity decreases from a theoretical maximum of 1.41 (ideal contact) to zero, as was shown in Ref. 2. Figure 1(b) (thick curve) shows the result for the case of an ideal contact. A study of this peak may thus be used to investigate the charge carrier injection conditions, and possible changes of these conditions during the operational lifetime.

The capacitance-peak has been observed for various systems,[2,8] and a quantitative analysis has been given in Ref. 2 for the case of hole-only devices based on a blue-emitting polyfluorene-triarylamine (PF-TAA) copolymer. However, within the model used to analyze the effect a constant mobility was

a)Electronic mail: w.c.germs@tue.nl.

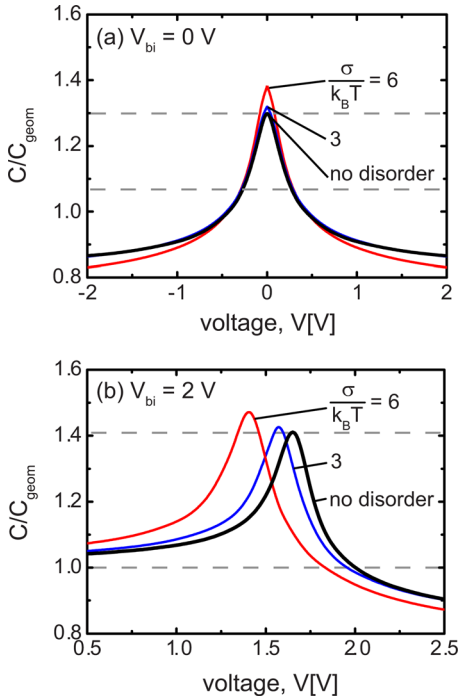

FIG. 1. Calculated $C(V)/C_{geom}$ curves for single-carrier devices with a thickness $L = 100$ nm, relative dielectric constant $\varepsilon_r = 3$, at $T = 300$ K and in the low-frequency limit, for (a) symmetric devices with ideal injection at both interfaces, so that $V_{bi} = 0$ V, and (b) asymmetric devices with ideal injection at one of the interfaces and a 2 eV injection barrier at the other interface, so that $V_{bi} = 2$ V. Thick curves show the results for the case of a constant mobility and diffusion coefficient ("no disorder," with peak heights indicated by horizontal dashed lines), and the thin curves show the results for transport within a spatially uncorrelated Gaussian density of states with a site density $N_t = 1 \times 10^{27}$ m^{-3} and a width $\sigma/(k_BT) = 3$ and 6.

assumed, whereas it was found in a subsequent study that the hole transport in PF-TAA is strongly affected by Gaussian energetic disorder.[9] In this paper, we show that the introduction of Gaussian disorder leads to a significant increase of the peak shift, $V_{bi} - V_{peak}$, for single-carrier and double-carrier devices, and to peak heights which are larger than for the case of a constant mobility and diffusion coefficient. The model used for calculating the frequency-dependent capacitance at any voltage is an extension of a recently developed one-dimensional Master-Equation OLED device model,[10] and employs a small-signal approach. Our findings can explain the 0.3 V difference between the value of V_{bi} for the above-mentioned PF-TAA based devices as obtained in Ref. 9 from measurements of current density versus voltage ($J(V)$) curves using the Extended Gaussian Disorder model (EGDM), and as obtained in Ref. 2 from $C(V)$ measurements assuming a constant mobility.

In Sec. II, the device model used for calculating the differential capacitance is discussed. In Sec. III, the disorder dependence of the capacitance peak height and position is discussed for single-carrier devices, and a comparison is made with experimental results obtained for PF-TAA based devices. In Sec. IV, a similar analysis is given for the case of double-carrier devices. It is furthermore shown that energetic disorder can lead to a negative differential capacitance, as has indeed been observed in various studies of double-carrier devices and for which various explanations were given in the literature.[11–15] Section V contains a summary and conclusions.

II. THEORETICAL MODEL

The systems studied are devices within which a single organic layer with thickness L is sandwiched between two metallic electrodes. The charge transport in the organic layer takes place by hopping in between sites at which the energies are spatially uncorrelated, with a Gaussian density of states characterized by a width σ and a hopping site density N_t. The complex impedance is calculated by applying a small-signal analysis method, within which a linearization approach is used to calculate the response of the system to a small applied voltage modulation.

As a first step, the steady-state solution of the drift-diffusion-recombination problem is calculated using a recently developed one-dimensional Master-Equation (1D-ME) OLED device model.[10] The model describes charge transport along a linear chain of N equidistant sites, with the electrodes at sites 0 and N. The steady-state current density across the interval m between sites $m-1$ and m is given by

$$J_{dc} = (c_{m-1,dc} r^{+}_{m,dc} - c_{m,dc} r^{-}_{m,dc}) \frac{e}{a^2}, \qquad (1)$$

with r^+ and r^- the forward and backward hopping rates, respectively, c the carrier concentration (occupation probability) at each site, e the elementary charge, and $a \equiv N_t^{-1/3}$ the average intersite distance in the organic semiconductor. The hopping rates depend on the local carrier density and electric field in a manner which is consistent with the mobility and diffusion coefficient as obtained within the EGDM.[3] The distance between the grid points used may be viewed as the effective hopping distance. It is close to a, but increases slightly with the dimensionless disorder parameter $\hat{\sigma} \equiv \sigma/(k_BT)$, with k_B the Boltzmann constant and T the temperature, as expected from percolation theory. The solution for a given applied voltage is obtained after iteration until a uniform current density is obtained. The injection barriers determine the boundary conditions, i.e., the values of c_0 and c_N. When no injection barrier is present, the Fermi level is at the top of the Gaussian DOS and the concentration is equal to 1/2. When an injection barrier Φ is present, the Fermi level at the interfacial site is taken at $-\Phi$ and the occupation is smaller than 1/2. We note that in the literature several alternative models describing the boundary conditions have been proposed.[17–21] However, the application of these models is restricted to systems with high injection barriers (injection limited current limit) and/or to systems without energetic disorder. Support for the approach described above was obtained from a comparison with the results of three-dimensional Master-Equation[22] or Monte Carlo[23] device simulations, carried out for a wide range of injection barriers and disorder parameters. For the case of PF-TAA based single-layer and single-carrier devices, the $J(V)$ curves as obtained from the 1D-ME model are in excellent agreement with the results from the continuum EGDM drift-diffusion model[9,24] which was used to deduce the parameter values describing the shape of the DOS. In double-carrier devices

the recombination rate in the limit of zero field is assumed to be given by the Langevin formula. For finite values of the field it is taken to be slightly larger, in a manner described in detail by Eq. (8) and Fig. 3 of Ref. 10 ("$k=4$ model").

The steady-state solution is fully characterized by the set of charge carrier concentrations $\{c_{m,dc}\}$ at all internal sites. The fields at all intersite intervals are equal to the sum of the effective applied field, $(V-V_{bi})/L$, and a contribution from the space charge in the device. The hopping rates depend only on the local carrier concentration and field. Within the small-signal approximation, the time (t) response to a small superimposed ac modulation voltage $\delta V = v_{ac}\exp(i\omega t)$ with angular frequency ω are an oscillatory ac current density $\delta J = \tilde{j}_{ac}\exp(i\omega t)$ and oscillatory local ac concentrations $\delta c_m = \tilde{c}_{ac,m}\exp(i\omega t)$. The tilde indicates that the concentration and current density amplitudes are complex, as they contain a phase factor. For single-carrier devices, the ac current density may be expressed as

$$J_{dc}+\delta J_m = [(c_{m-1,dc}+\delta c_{m-1})(r_m^+ + \delta r_m^+) - (c_{m,dc}+\delta c_m)(r_m^- + \delta r_m^-)]\frac{e}{a^2} + \varepsilon\frac{dF_m}{dt}, \quad (2)$$

where the final term is the displacement contribution. Writing $\delta r_m^{+(-)} = \tilde{r}_{ac,m}^{+(-)}\exp(i\omega t)$, it follows after linearization of Eq. (2) and after elimination of the steady-state contribution that the local current density amplitudes are given by

$$\tilde{j}_{ac,m} = (r_{m,dc}^+\tilde{c}_{ac,m-1} - r_{m,dc}^-\tilde{c}_{ac,m} + c_{m-1,dc}\tilde{r}_m^+ - c_{m,dc}\tilde{r}_m^-)\frac{e}{a^2} + i\omega\varepsilon\left(\sum_{k=1}^{N-1}\frac{dF_m}{dc_k}\tilde{c}_{ac,k} + \frac{\tilde{v}_{ac}}{L}\right). \quad (3)$$

The ac amplitudes of the hopping rates are given by

$$\tilde{r}_m^+ = \frac{dr_m^+}{dc_{m-1}}\tilde{c}_{ac,m-1} + \frac{dr_m^+}{dF_m}\sum_{k=1}^{N-1}\left(\frac{dF_m}{dc_k}\tilde{c}_{ac,k} + \frac{\tilde{v}_{ac}}{L}\right) \quad (4)$$

and

$$\tilde{r}_m^- = \frac{dr_m^-}{dc_m}\tilde{c}_{ac,m} + \frac{dr_m^-}{dF_m}\sum_{k=1}^{N-1}\left(\frac{dF_m}{dc_k}\tilde{c}_{ac,k} + \frac{\tilde{v}_{ac}}{L}\right). \quad (5)$$

The first terms in Eqs. (4) and (5) arise as a result of the charge carrier concentration dependence of the mobility. The second terms are due to the dependence of the hopping rates on the local field, and contain contributions from the ac space charge throughout the device and from the applied ac voltage. The concentration and field derivatives are calculated at the dc values of the local concentration and the field, respectively. The requirement that the ac current density amplitudes $\tilde{j}_{ac,m}$ are equal for all intervals leads to a set of N equations (Eq. (3)) which are linear in the concentrations $\tilde{c}_{ac,m}$. The coefficients are straightforwardly calculated using the formalism developed in Ref. 10. Solving this set of N equations provides the values of $\tilde{c}_{ac,m}$ for $1 \le m \le N-1$, as well as $\tilde{j}_{ac}$. The differential conductance G and the differential capacitance C are then obtained from the admittance, which is defined as

$$Y \equiv \frac{\delta J}{\delta V} = \frac{\tilde{j}_{ac}}{v_{ac}} = G + i\omega C. \quad (6)$$

An analogous method is used for deriving the capacitance of double-carrier devices. The $2(N-1)$ electron and hole ac concentration amplitudes at the inner sites and the ac current density amplitude are determined from a set of $2N-1$ linear equations, obtained from the requirement that the ac current density in all N intervals is equal and the requirement of charge conservation upon recombination at each of the $N-1$ internal sites.

III. SINGLE-CARRIER DEVICES

A. Simulation results

Using the model developed in the previous section, we calculated the voltage dependence of the capacitance of a system formed by an organic semiconductor sandwiched between two metallic electrodes, and varied the disorder parameter. Figure 1(a) includes the low-frequency $C(V)$ curves for single-carrier devices at $T=300\,\mathrm{K}$ with a layer thickness $L=100\,\mathrm{nm}$, for $V_{bi}=0\,\mathrm{V}$, $N_t=10^{27}\,\mathrm{m}^{-3}$, a relative dielectric constant $\varepsilon_r=3$, and no injection barriers, for the cases $\sigma/(k_BT)=3$ and 6. Figure 1(b) includes the results of otherwise identical devices for the case $V_{bi}=2\,\mathrm{V}$. The frequency is chosen in the low-frequency limit, equal to 10^{-15} Hz, far below the frequency above which the capacitance becomes frequency dependent. There is no practical limit imposed by the method to how low the frequency can be chosen.

The figures show that the peak height increases with increasing disorder parameter, and that it exceeds the values obtained for the case of a constant mobility. We find that for large V_{bi} the peak voltage follows the built-in voltage, as for the case of a constant mobility, but at a distance which increases with increasing disorder parameter. V_{peak} shifts from 1.65 V (constant mobility) to 1.57 V for $\sigma/(k_BT)=3$ and to 1.41 V for $\sigma/(k_BT)=6$. The observed increase of the peak height and peak shift with respect to V_{bi} indicate that with increasing disorder the role of diffusion becomes more important. This can be explained as a result of the disorder and charge carrier concentration dependent enhancement of the diffusion coefficient, described by the generalized Einstein equation.[16] The diffusion coefficient enhancement results in a redistribution of the carrier density in the device, as may be seen from the simulation results for comparable devices shown in Fig. 4 in Ref. 24.

In Ref. 2, it was shown that in the absence of disorder, V_{peak} and C_{peak} depend only on the dimensionless carrier densities at the electrodes

$$\gamma_i = \frac{e^2L^2}{\varepsilon k_BT}n_i, \quad (7)$$

with n_i (for $i=1, 2$) the carrier density at the injecting and exit electrodes. The factor which is used to normalize the carrier density is (apart from a numerical factor) equal to the carrier density in the device center at zero voltage and for the

case of ideal contacts. For the case of such an ideal symmetric device, the γ-parameters are thus a dimensionless measure of the role of charge carrier diffusion from the electrodes toward the device center. For the case of an asymmetric device such as discussed in Fig. 2, with a large-built-in voltage resulting from a small and a large barrier at the injecting and exit electrodes, respectively, V_{peak} is only determined by γ_1 and increases then with decreasing γ_1 (see Eq. (1) in Ref. 2) This may be understood from the decreasing role of carrier diffusion from the injecting contact, so that the current density onset voltage (and hence V_{peak}) shifts to a higher value, more close to V_{bi}. In such a case, V_{peak} increases with a decrease of the layer thickness or an increase of the barrier at the injecting contact. Figures 2(a) and 2(c) show that, qualitatively, such a trend is also obtained in the presence of energetic disorder, studied for systems with $V_{bi} = 2$ V. The effect of the boundary conditions on the peak height is somewhat more complicated, as may be seen from Fig. 3(c) in Ref. 2, which reveals that for a strongly asymmetric device C_{peak} can decrease with increasing thickness and with an increase of the injection barriers at both interfaces. Figures 2(b) and 2(d) show that such trends are also obtained in the presence of energetic disorder.

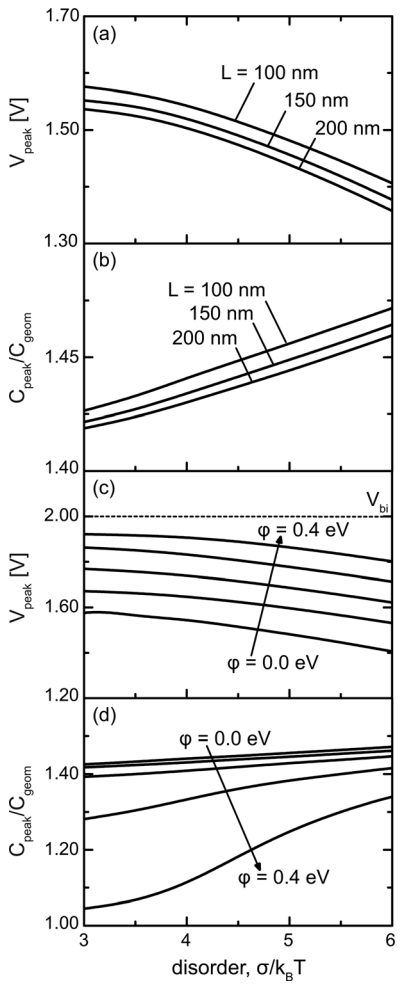

FIG. 2. Calculated effect on the disorder dependent peak voltage and peak height due to (a),(b) a variation of the layer thickness and (c),(d) a variation in the injection barrier, in all cases for devices studied in Fig. 1(b). The layer thickness and injection barrier are varied in 50 nm and 0.1 eV steps, respectively.

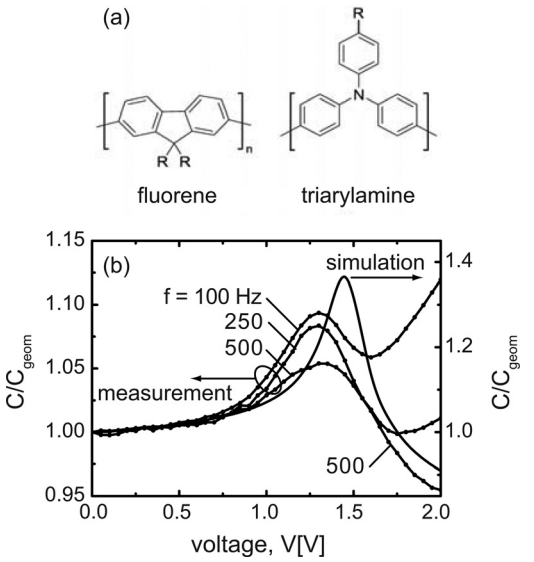

FIG. 3. (a) The structure of the PF and TAA monomer units. (b) $C(V)$ curves for PEDOT:PSS |97 nm PF – TAA(7.5%)| Pd devices, measured at room temperature at various frequencies (left-hand scale) and simulated in the low-frequency limit (right-hand scale). The structure of the PF and TAA monomer units is shown as an inset. The simulation was carried out using $\sigma = 0.13$ eV, $N_t = 0.6 \times 10^{27}$ m^{-3}, $V_{bi} = 1.95$ eV, and $\varepsilon_r = 3.2$.

B. Comparison with experiment

We apply the model to the PF-TAA based hole-only devices, already discussed in the Introduction, for which the $C(V)$ curve was analyzed in Ref. 2 assuming a constant mobility and diffusion coefficient. The hole-injecting layer is poly(3,4-ethylenedioxythiophene):poly(styrene sulfonic acid) (PEDOT:PSS), fabricated by spin-coating on a 100 nm indium-tin-oxide (ITO) layer on glass, while an evaporation deposited Pd cathode layer was used. The device structure is thus PEDOT:PSS |PF – TAA| Pd. The experimental method has been described in Ref. 2. The structure of the monomer units is shown in Fig. 3(a). The triarylamine units are randomly copolymerized with the fluorene units, and are present with a concentration of 7.5 mol %. With increasing TAA concentration, the mobility first decreases, when these units act as hole traps. A steep increase is observed beyond a TAA-concentration of approximately 2%, above which the transport takes place via the TAA units (with an ionization potential of approximately 5.1 eV), instead of via the polyfluorene highest occupied molecular orbitals (HOMO), at approximately 5.8 eV.[25] As the ionization potential of PEDOT:PSS is approximately 5.1 eV, a large (~0.7 eV) injection barrier to the PF-HOMO states is present at the interface, so that the space charge density at the interface, related to the occupation of the PF-states, is expected to be very small. This explains why for PEDOT:PSS/PSF devices, containing poly(spirofluorene) (PSF) which is electronically very similar to PF and which contains no TAA units, no peak in the low-frequency differential capacitance has been observed.[8]

Figure 3(b) shows for the PEDOT:PSS |97 nm PF – TAA(7.5%)| Pd hole-only devices a series of $C(V)$ curves measured at low frequencies, taken from Ref. 2 (left axis, using the capacitance measured at $V = 0$ V, $C_{V=0}$, for

normalizing the curve), and the simulated curve, obtained using the experimental parameters given in the figure caption (right axis). The parameters describing the hole density of states and the hopping mobility were taken from the analysis of the steady-state $J(V)$ curves, carried out in Ref. 9 within the EGDM for a wide range of layer thicknesses and temperatures. No evidence for the presence of spatially correlated (instead of random) energetic disorder was found.[25] No injection barrier at the PEDOT:PSS interface was assumed, consistent with the excellent energy level alignment of the PEDOT:PSS electrode layer and the HOMO energy of the TAA units, as mentioned above. The analysis led to $V_{bi} = 1.95$ eV, a value which is much larger than would be expected on the basis of the vacuum work function of the Pd cathode. This points at the formation of a significant interfacial dipole layer.

Both curves show a distinct shift of V_{peak} to a value below V_{bi}. The measurement shows a peak at 1.3 V, approximately 0.65 V below V_{bi}, whereas the simulation leads to $V_{peak} \cong 1.45$ V, corresponding to a peak shift of approximately 0.5 V. In view of the experimental uncertainty in the parameters used in the model calculation (± 0.05 V for V_{bi} and ± 0.01 eV for σ, as stated in Ref. 9, the agreement may be regarded as good.

We remark that a recent experimental study of the same devices,[26] carried out approximately two years after the work reported in Refs. 2 and 9, confirmed the values of the bulk transport parameters used and the approximately 0.65 V difference between V_{bi} and V_{peak}, but revealed an approximately 0.3 V decrease of both voltages. This was attributed to a small time-dependent change of the dipole layer at the PF-TAA/Pd interfaces. As expected from the simulations, such a change has no effect on the peak shift. We also note that the same study revealed that V_{peak} is very close to the voltage at which the signal as obtained from an electroabsorption (EA) experiment goes through zero (zero field-voltage, $V_{0,EA}$), and that for these devices $V_{0,EA}$ is consistent with predictions as obtained from an EGDM simulation. It was furthermore found that both voltages may be interpreted as an effective current density onset voltage.

The height of the experimental low-frequency capacitance peak shown in Fig. 3(b) is significantly (approximately a factor of three) smaller than as obtained from the simulation, and it is somewhat broader. Furthermore, the simulated capacitance decreases above the peak voltage to a value of 0.80 C_{geom} at high voltages, whereas the experimental capacitance increases at high voltages with a rate which is larger for smaller frequencies. The smaller peak height and large peak width may, in part, be explained as a result of small lateral variations of the built-in voltage. The increase of the capacitance at higher voltages can be attributed to charge carrier relaxation. This is a low-frequency contribution to the capacitance for which a phenomenological description was given by Martens *et al.*[1] for the case of poly(*p*-phenylene vinylene) based devices. The effect is due to the effective time (or frequency) dependence of the mobility which arises in any transient experiment, in which after a sudden change of the carrier density in a certain volume the local energy distribution is not immediately equal to the steady-state distribution. The effect of charge carrier relaxation on the capacitance is expected to increase with increasing space charge, and hence with increasing voltage, consistent with the experimental results. Modeling of the effect of charge carrier relaxation on the capacitance within the framework of the EGDM shows that including the effect hardly affects V_{peak}, but that it can lead to a slight decrease of the peak height.[27]

Another possible explanation of the reduced peak height would be the presence of an injection barrier at the PEDOT:PSS/PF-TAA interface. However, we find that a significant effect on the peak height is only expected when the injection barrier is at least 0.3 V, as also suggested by the simulation results shown in Fig. 2(d) for a system described by similar parameters, and that the introduction of such a barrier would give rise to a strong upward peak shift which is inconsistent with the measured value. We remark that it is, in fact, remarkable that from the analyses of the $J(V)$ and EA measurements no evidence for a (significant) injection barrier was found. It is well known, e.g., from an extensive study of metal/semiconductor/metal devices with aluminum-tris-(8-hydroxy-quinoline) (Alq_3) as the organic semiconductor,[28] that in the case of excellent energy level alignment an effective injection barrier can arise as a result of charge transfer to the organic layer, leading to the formation of a dipole layer. Such an effect has indeed been obtained from phenomenological modeling, involving image charge stabilization of a dipole layer,[29] as well as from *ab initio* modeling using density functional theory (see, e.g., Ref. 30). On the other hand, experimental evidence of strongly weakened dipole layer formation at interfaces with PEDOT:PSS has been found by Tengstedt *et al.*[31] Indeed, a weakening of image charge interactions might be expected from the structure of PEDOT:PSS, which is an inhomogeneous material consisting of conducting PEDOT segments in a matrix of non-conducting PSS, which is known to segregate to the surface.[32] The complex structure of PEDOT:PSS has been shown to give rise to anisotropic conduction.[33] The decreased height of the $C(V)$ peak suggests that it might be of interest to develop a refined model for simulating the hole injection at the PEDOT:PSS/PF-TAA interface, taking the effect of the inhomogeneous character of the PEDOT:PSS layer on the charge carrier density in PF-TAA at the interface with PEDOT:PSS layer into account.

IV. DOUBLE-CARRIER DEVICES

Figure 4(a) shows simulated low-frequency $C(V)$ curves for 100 nm double-carrier devices which are otherwise identical to the single-carrier devices studied in Fig. 1(a) (no injection barriers, the same electron and hole mobility functions and $V_{bi} = 2$ V). The voltage differences between V_{peak} and V_{bi} increase with increasing disorder parameter, and are approximately a factor of two larger than for corresponding single-carrier devices, as may be seen from a comparison given in Fig. 4(b). Furthermore, the peak heights (also shown in Fig. 4(b)) are almost a factor of two larger. These results reflect the larger role of charge carrier diffusion in the double-carrier devices, in which due to diffusion near both interfaces a high charge density is present. The result is

consistent with the current onset difference between otherwise identical single-carrier and double-carrier devices with varying Gaussian disorder, displayed in Fig. 4 of Ref. 10.

Figure 4(c) shows the effect of the introduction of an electron injection barrier, ϕ_e, on the $C(V)$ curves, for otherwise identical devices with $\sigma/(k_BT) = 3$. The built-in voltage is equal to $E_g - \phi_e$, where E_g is the 2 eV gap energy taken. The figure shows clearly that the peak voltage varies nonlinearly with V_{bi}. In general, deducing the built-in voltage from the peak voltage will therefore require detailed device modeling. However, when the electron injection barrier is sufficiently large, so that the space charge density near the cathode is very small, no detailed modeling is needed for deducing injection barrier *differences*, as these are then equal to the measured peak voltage differences. This condition is met for the $\phi_e = 0.5$ and 0.7 eV cases studied, for which Fig. 4(c) reveals a shift of the peak voltage from 1.07 to 0.87 V. Furthermore, under these conditions the peak shift is seen to be very close to the peak shift for the corresponding single-carrier device (~0.42 V). If this peak shift is known from experiments and modeling of single-carrier devices (ΔV_{SC}), the built-in voltage for the double-carrier device follows then from the measured peak voltage using

$$V_{bi,DC} = V_{peak,DC} + \Delta V_{SC}. \quad (8)$$

This is a general result, irrespective of the disorder parameter.

As an application, Fig. 5 shows the measured low-frequency $C(V)$ curves for PF-TAA(7.5%) based double-carrier devices with Ba/Al and LiF/Ca/Al cathodes. Figure 5(a) gives the energy level scheme. The barrier from the LiF/Ca/Al and Ba/Al cathodes to the lowest-occupied molecular orbital states of the copolymer, which are PF-derived, is approximately 0.4 and 0.5 eV, respectively (see below). For the case of a BaAl cathode (see Fig. 5(b)), a pronounced peak in the capacitance is observed at 2.39 V. Under the assumption that the barrier at the Ba/Al interface is sufficiently high, the ~0.65 eV peak shift as observed from the analysis of single-carrier device experiments would imply that $V_{bi,dc} \cong 3.04$ eV. The somewhat smaller shift of ~0.50 V as obtained from the single-carrier device simulations would imply that $V_{bi,dc} \cong 2.89$ eV. Replacement of the Ba/Al cathode by a LiF/Ca/Al cathode is known to give rise to enhanced electron injection.[34] The 0.13 eV higher peak voltage obtained for these devices, as shown in Fig. 5(c), implies that the injection barrier is 0.13 eV smaller than for Ba/Al electrodes, provided that for both electrodes the injection barrier is sufficiently large. The appropriateness of the latter criterion is supported by recent analyses of the steady-state current-voltage curves of single-carrier

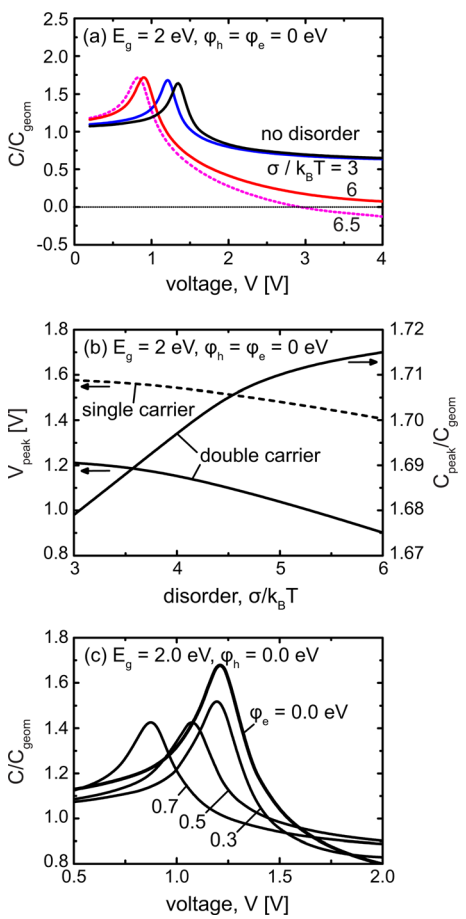

FIG. 4. (a) Calculated $C(V)/C_{geom}$ curves for double-carrier devices with based on a semiconductor with a gap energy $E_g = 2$ eV, a thickness $L = 100$ nm, relative dielectric constant $\varepsilon_r = 3$, at $T = 300$ K and in the low-frequency limit. The contacts are ideal, so that $V_{bi} = 2$ V. (b) Calculated dependence of the peak voltage and the peak capacitance on the disorder parameter, for the devices studied in figure (a). (c) Calculated effect of a finite electron injection barrier on the $C(V)/C_{geom}$ curves for devices which are otherwise identical to those studied in (a).

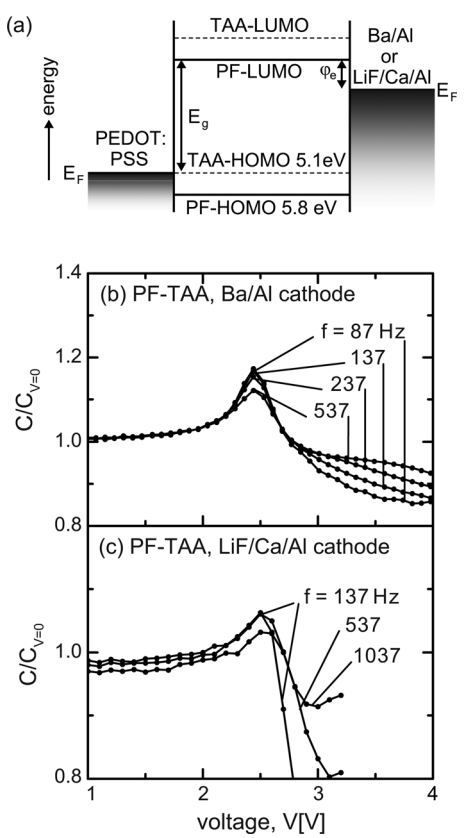

FIG. 5. (a) Energy-level structure for the PF-TAA devices studied, and $C(V)$ curves measured at room temperature at various frequencies for (b) PEDOT:PSS |101 nm PF – TAA(7.5%)| Ba |Al devices and for (c) PEDOT:PSS| 96 nm PF-TAA(7.5%) |LiF|Ca| Al devices.

electron-only and double-carrier PF-TAA(7.5%)/LiF/Ca/Al-based devices, which yielded $\phi_e = 0.30 \pm 0.10$ eV (Ref. 35) and $\phi_e \cong 0.40$ eV,[36] respectively. Using the latter value, the analysis of the $C(V)$ curves would imply that for the Ba/Al devices $\phi_e \cong 0.53$ eV.

Figure 4(a) shows a strong disorder-related decrease of the capacitance for voltages beyond the capacitance peak, even to negative values for disorder parameters $\sigma/(k_BT) \gtrsim 6$. A negative differential capacitance (NDC) at voltages close to the built-in voltage has been reported from several studies of double-carrier devices.[11–15] These studies suggest that the effect results from the presence of a high-density nearly charge-compensated electron hole plasma in such devices. Various quantitative models have been proposed, involving a strong (more than one order of magnitude) reduction of the bimolecular recombination rate near the electrode interfaces,[12] a non-equilibrium population of interface trap states,[14] and trap-mediated recombination.[15] Our simulation method can thus already account for the occurrence of a NDC, provided that sufficient energetic disorder is present.

We find that the capacitance at high voltages and low frequencies of the double-carrier devices studied in Fig. 4(a) is very sensitive to the recombination rate assumed. E.g., for the case $\sigma/(k_BT) = 3$ or 6 a reduction of the recombination rate by a factor of 2.5 already reduces the capacitance to approximately zero or $-2.3\ C_{geom}$, respectively. Although it has been proposed that the recombination rate in organic semiconductors can be much smaller than as given by the Langevin formula,[12] recent Monte Carlo calculations have indicated that the Langevin formula holds well, albeit that it should be applied using so-called "bipolar" mobilities. In double-carrier devices the mobility is smaller than the single-carrier mobility due to the interaction with the randomly distributed carriers of the other type.[23] A quantitative analysis for specific systems should thus include the effect of Coulomb-interactions on the charge carrier mobility and recombination rate.[23] Furthermore, also the role of electron trap states, at which hole capture followed by recombination can take place, should be taken into account.[35,37,38] Giving such an analysis, and an analysis of the positive relaxation contribution at high voltages which is revealed by the experimental double-carrier $C(V)$ curves given in Fig. 5, would be beyond the scope of this paper.

V. SUMMARY AND CONCLUSIONS

A one-dimensional master equation model for transient charge transport has been developed that takes disorder into account according to the Extended Gaussian Disorder model. The current response to an infinitesimal oscillation on a dc voltage is calculated using the small signal approximation. Subsequently, the differential capacitance is calculated and used to study the influence of disorder on the peak in the differential capacitance versus voltage curve, which can be used to determine the injection barriers in OLEDs. The model showed a pronounced disorder dependence in the peak position and height, which indicates that disorder cannot be neglected when this peak is used to determine the injection barriers. The capacitance peak voltage is more strongly shifted to a value below the built-in voltage than as expected in the absence of disorder. The shift is explained by the significant diffusion current below the built-in voltage, which becomes even more important with increasing disorder. For double-carrier devices, the peak in the $C(V)$ curve is shifted to lower voltages than for single-carrier devices, which is explained as a result of the increased charge carrier concentration giving rise to an enhanced diffusion current density and a reduced onset voltage.

For a small injection barrier at one of the contacts, a change in the barrier leads to a nonlinear shift in the peak voltage. Deducing the built-in from this type of measurements therefore requires detailed device modeling. Only at sufficiently large injection barriers, the built-in voltage varies linearly with the peak voltage. The model is applied successfully to single-carrier and double-carrier devices based on the blue-emitting polymer PF-TAA.

For double-carrier devices based on materials with a large width of the Gaussian density of states, the model also revealed a negative capacitance at voltages above V_{peak}. This indicates that disorder is one of the important parameters determining the observation of a negative capacitance. For single-carriers a negative capacitance was not found, consistent with the fact that the effect has (so far) only been observed in some double-carrier devices. We remark that in actual organic semiconductors the electron transport is often described by a more complex shape of the density of states, formed by a Gaussian and a superimposed exponential trap density of states. Future modeling studies of the negative capacitance should include this more refined description of the DOS.

At voltages well beyond the low-frequency capacitance peak the model starts to break down. The experimental capacitance shows then often a strong increase with the voltage, to values well above the geometrical capacitance. This effect is due to relaxation of injected charge carriers, related to the presence of energetic disorder, which is not taken into account in this work. For the case of single-carrier devices, an extension of the model to include this effect has been recently developed.[27]

ACKNOWLEDGMENTS

The authors would like to thank A. J. M. van den Biggelaar for skillful sample preparation, and Sumation Co., Ltd for the supply of Lumation™ Blue Series polymers. This research has received funding from the Dutch Technology Foundation STW (VIDI Grant No. 07575, W.Chr.G.), the Dutch nanotechnology program NanoNed (contribution S.L.M.v.M.), and from the European Community's Program No. FP7-213708 (AEVIOM, contribution R.C.), and this work forms part of the research program of the Dutch Polymer Institute (Project #680).

[1] H. C. F. Martens, H. B. Brom, and P. W. M. Blom, Phys. Rev. B **60**, R8489 (1999).
[2] S. L. M. van Mensfoort and R. Coehoorn, Phys. Rev. Lett. **100**, 086802 (2008).
[3] W. F. Pasveer, J. Cottaar, C. Tanase, R. Coehoorn, P. A. Bobbert, P. W. M. Blom, D. M. de Leeuw, and M. A. J. Michels, Phys. Rev. Lett. **94**, 206601 (2005).

[4]J. Zhou, Y. C. Zhou, J. M. Zhao, C. Q. Wu, X. M. Ding, and X. Y. Hou, Phys. Rev. B **75**, 153201 (2007).
[5]R. Coehoorn, W. F. Pasveer, P. A. Bobbert, and M. A. J. Michels, Phys. Rev. B **72**, 155206 (2005).
[6]The exact expression is $C_{peak}/C_{geom} = \pi^2/3\text{-}2$ (R. Coehoorn, unpublished).
[7]R. Kassing, Phys. Status Solidi A **28**, 107 (1975).
[8]A. van Dijken, A. Perro, E. A. Meulenkamp, and K. Brunner, Org. Electron. **4**, 131 (2003).
[9]S. L. M. van Mensfoort, S. I. E. Vulto, R. A. J. Janssen, and R. Coehoorn, Phys. Rev. B **78**, 085208 (2008).
[10]R. Coehoorn and S. L. M. van Mensfoort, Phys. Rev. B **80**, 085302 (2009).
[11]I. N. Hulea, R. F. J. van der Scheer, H. B. Brom, B. M. W. Langeveld-Voss, A. van Dijken, and K. Brunner, Appl. Phys. Lett. **83**, 1246 (2003).
[12]H. H. P. Gommans, M. Kemerink, and R. A. J. Janssen, Phys. Rev. B **72**, 235204 (2005).
[13]N. D. Nguyen, M. Schmeits, and P. Loebl, Phys. Rev. B **75**, 075307 (2007).
[14]J. Bisquert, G. Garcia Belmonte, A. Pitarch, and H. J. Bolink, Chem. Phys. Lett. **422**, 184 (2006).
[15]E. Ehrenfreund, C. Lungenschied, G. Dennler, H. Neugebauer, and N. S. Sariciftci, Appl. Phys. Lett. **91**, 012112 (2007).
[16]Y. Roichmann and N. Tessler, Appl. Phys. Lett. **80**, 1948 (2002).
[17]V. I. Arkhipov, E. V. Emelianova, Y. H. Tak, and H. Baessler, J. Appl. Phys. **84**, 848 (1998).
[18]J. C. Scott and G. G. Malliaras, Chem. Phys. Lett. **299**, 115 (1999).
[19]Y. Shen, M. W. Klein, D. B. Jacobs, J. C. Scott, and G. G. Malliaras, Phys. Rev. Lett. **86**, 3867 (2001).
[20]M. A. Baldo and S. R. Forrest, Phys. Rev. B **64**, 085201 (2001).
[21]P. L. Bullejos, J. A. Jimenez Tegada, M. J. Deen, O. Marinov, and W. R. Datars, J. Appl. Phys. **103**, 064504 (2008).
[22]J. J. M. van der Holst, M. A. Uijttewaal, B. Ramachandhran, R. Coehoorn, P. A. Bobbert, G. A. de Wijs, and R. A. de Groot, Phys. Rev. B **79**, 085203 (2009).
[23]J. J. M. van der Holst, F. W. A. van Oost, R. Coehoorn, and P. A. Bobbert, Phys. Rev. B **80**, 23202 (2009).
[24]S. L. M. van Mensfoort and R. Coehoorn, Phys. Rev. B **78**, 085207 (2008).
[25]R. J. de Vries, S. L. M. van Mensfoort, V. Shabro, R. A. J. Janssen, and R. Coehoorn, Appl. Phys. Lett. **94**, 163307 (2009).
[26]R. J. de Vries, S. L. M. van Mensfoort, R. A. J. Janssen, and R. Coehoorn, Phys. Rev. B **81**, 125203 (2010).
[27]W. C. Germs, J. J. M. van der Holst, S. L. M. van Mensfoort, P. A. Bobbert, and R. Coehoorn, Phys. Rev. B **84**, 165210 (2011).
[28]I. H. Campbell and D. L. Smith, Appl. Phys. Lett. **74**, 561 (1999).
[29]E. Tutiš, M.-N. Bussac, and L. Zuppiroli, Appl. Phys. Lett. **75**, 3880 (1999).
[30]P. C. Rusu, G. Giovannetti, C. Weijtens, R. Coehoorn, and G. Brocks, Phys. Rev. B **81**, 125403 (2009), and references therein.
[31]C. Tengstedt, W. Osikowicz, W. Salaneck, I. D. Parker, C.-H. Hsu, and M. Fahlman, Appl. Phys. Lett. **88**, 053502 (2006).
[32]M. M. de Kok, M. Buechel, S. I. E. Vulto, P. van de Weijer, E. A. Meulenkamp, S. H. P. M. de Winter, A. J. G. Mank, H. J. M. Vorstenbosch, C. H. L. Weijtens, and V. van Elsbergen, Phys. Status Solidi A **201**, 1342 (2004).
[33]A. M. Nardes, M. Kemerink, and R. A. J. Janssen, Phys. Rev. B **76**, 085208 (2007).
[34]R. Coehoorn, S. Vulto, S. L. M. van Mensfoort, J. Billen, M. Bartyzel, H. Greiner, and R. Assent, Proc. SPIE **6192**, 61920O (2006).
[35]S. L. M. van Mensfoort, J. Billen, S. I. E. Vulto, R. A. J. Janssen, and R. Coehoorn, Phys. Rev. B **80**, 033202 (2009).
[36]S. L. M. van Mensfoort, J. Billen, S. I. E. Vulto, R. A. J. Janssen, and R. Coehoorn, J. Appl. Phys. **109**, 064502 (2011).
[37]M. M. Mandoc, B. de Boer, and P. W. M. Blom, Phys. Rev. B **73**, 155205 (2006).
[38]G. A. H. Wetzelaer, M. Kuik, H. T. Nicolai, and P. W. M. Blom, Phys. Rev. B **83**, 165204 (2011).